Desalination 454 (2019) 48–58

Contents lists available at ScienceDirect

Desalination

journal homepage: www.elsevier.com/locate/desal

Thin film nanocomposite reverse osmosis membrane modified by two dimensional laminar MoS_2 with improved desalination performance and fouling-resistant characteristics

Yi Li[a,b,c], Shishi Yang[a,b], Kaisong Zhang[a,*], Bart Van der Bruggen[c,d,**]

[a] Key Laboratory of Urban Pollutant Conversion, Institute of Urban Environment, Chinese Academy of Sciences, Xiamen 361021, PR China
[b] University of Chinese Academy of Sciences, Beijing 100049, PR China
[c] Department of Chemical Engineering, KU Leuven, Celestijnenlaan 200F, B-3001 Leuven, Belgium
[d] Faculty of Engineering and the Built Environment, Tshwane University of Technology, Pretoria, South Africa

GRAPHICAL ABSTRACT

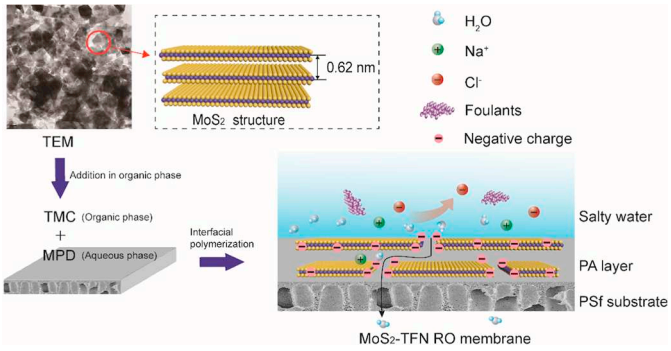

ARTICLE INFO

Keywords:
Two-dimensional (2D) nanomaterial
Reverse osmosis membrane
Thin film nanocomposite (TFN)
Desalination
Antifouling

ABSTRACT

Two dimensional (2 D) layered materials with special properties provide opportunities to design energy-efficient membranes for water desalination. A negatively charged layered graphene analogue, molybdenum disulfide (MoS_2) was synthesized through liquid exfoliation. A novel thin film nanocomposite (TFN) reverse osmosis (RO) membrane was successfully fabricated with prepared laminar MoS_2 as fillers in the organic phase through interfacial polymerization of *m*-phenylenediamine and trimesoyl chloride monomers. The laminar MoS_2 nanosheets were observed by transmission electron microscopy (TEM), and the nanosheets were dispersed in the polyamide (PA) matrix as well as on the membrane surface. The properties of the resultant TFN membranes were effectively modified by taking the advantage of two dimensional features, i.e., the negative charge and the hydrophilic sites of layered MoS_2. Compared to a classical TFC membrane, the MoS_2 incorporated TFN membranes were found to have an increased salt rejection and higher water flux. Moreover, 0.01 wt% MoS_2-TFN membrane showed a superior fouling resistance against proteins as foulants. The antifouling behavior of this

* Correspondence to: K. Zhang, Key Laboratory of Urban Pollutant Conversion, Institute of Urban Environment, Chinese Academy of Sciences, Xiamen, 361021, PR China.
** Correspondence to: B. Van der Bruggen, Department of Chemical Engineering, KU Leuven, Celestijnenlaan 200F, B-3001 Leuven, Belgium; Faculty of Engineering and the Built Environment, Tshwane University of Technology, Pretoria, South Africa.
E-mail addresses: kszhang@iue.ac.cn (K. Zhang), bart.vanderbruggen@cit.kuleuven.be (B. Van der Bruggen).

https://doi.org/10.1016/j.desal.2018.12.016
Received 11 June 2018; Received in revised form 21 December 2018; Accepted 22 December 2018
Available online 29 December 2018

TFN membrane was observed by field-emission scanning electron microscopy (FE-SEM). Stability tests demonstrated that there was a loss of MoS_2 in the initial 2 h filtration, but the process is stable in the long-term.

1. Introduction

Reverse osmosis (RO) desalination technology is one of the most effective approaches for addressing the worldwide water scarcity by producing fresh water from sea water, groundwater and other wastewater sources [1,2]. However, the required energy consumption when using traditional polymeric thin-film composite (TFC) aromatic polyamide (PA) membranes is relatively high, and the process is constrained by several challenges including limited water flux, insufficient salt rejection and an inferior fouling resistance. Highly permselective and inexpensive antifouling RO membranes are required in order to reduce the cost and energy input associated with water desalination [3].

Two dimensional (2D) nanomaterials are a diverse and largely underexploited source with outstanding properties, with attractive interests as catalysts, and in optoelectronics. One representative 2D nanomaterial, graphene oxide (GO) nanosheets, showed a great potential in water desalination and separation applications due to its atomic thickness, mechanical properties, multifunctional groups and the capability of providing extremely fast water channels. GO with size of micrometers was used in the development of new membranes, which have a water flux (10^4–10^5 L m^{-2} day^{-1} bar^{-1}) of several orders of magnitude higher than commercial RO membranes [4]. However, their use is restricted by the low salt rejections (< 90%) [5,6]. Nevertheless, assembling GO nanosheets on the surface of an RO membrane might enhance the antifouling properties and chlorine resistance of the membrane, while maintaining the separation performance. Alternatively, GO was mainly used as functional material in tailoring PA-TFC RO membranes both on the surface selective layer and in the substrate, through an in-situ modification method. A PA-TFC RO membrane fabricated on a GO incorporated sublayer was found to have a water flux 1.6–4 times higher than that of a commercial RO membrane [7]. Embedding of GO in the surface active layer also promotes the water flux, in the range of 20%–60%, and retain the salt rejections [8]. The properties of a TFN RO membrane were also modified by 2D nano clay with the advantage of their unique charge properties and hydrophilic nature [9]. Both negatively and positively charged clay nanomaterial filled TFN membranes showed an increased hydrophilicity and an improved desalination performance. Thus, atomically thickness 2D layered materials open a new way for tailoring the membrane structure, mechanical strength, surface hydrophilicity, surface charge, charge density and surface roughness in the PA skin layer [10,11]. TFN RO membranes modified with 2D nanomaterial may represent the next generation of high-performance RO membranes in water desalination [10].

Newly developed 2 D materials such as molybdenum disulfide (MoS_2) [12–14], WS2 [15], h-Boron nitride (BN) nanosheets [16,17] and titanium carbide ($Ti_3C_2T_x$) [18] may have potential in water separation and purification. MoS_2 is a prototypical transition metal dichalcogenides (TMD), which is made up of hexagonal layers of Mo and S atoms. MoS_2 layers have a sandwich structure with molybdenum atoms arranged between two sulphur sheets, as depicted in Fig. 1. The distance of two Mo atoms in vicinal MoS_2 layers is ~0.62 nm with laminar channels space of ~0.29 nm, which is smaller than the kinetic diameter of salt ions, such as Na^+ (0.716 nm) and Cl^- (0.664 nm), and is slightly larger than water molecules (0.276 nm). Mono- or few- layered MoS_2 nanosheets can be easily obtained from exfoliating of bulk MoS_2 crystals [19–21]. Molecular dynamics (MD) simulations suggested that a single-layer MoS_2 with a nanopore area of 20–60 Å^2 can effectively reject 88% of salt ions [14] and the hydrophilic sites at the edge of the nanopores could also give rise to the attraction of water molecules, which enhances the water permeation rate by five orders of magnitude [13]. Membranes assembled from atom-thick MoS_2 sheets through vacuum filtration technique exhibited a 3–5 times higher water permeance than GO membranes [12]. It was observed that all sulphur atoms were exposed on both sides of MoS_2 monolayer [22], which makes the surface of the MoS_2 sheets hydrophilic and provides a high affinity to water through hydrogen bonding [12]. Despite these simulation and experimental efforts, some significant technical difficulties remain, including the preparation of a large area of monolayer MoS_2 and generating nanopores with controllable size on the MoS_2 nanosheets. These are strong impediments for real-world water desalination applications. Alternatively, due to the highly negatively charged properties and the hydrophilic sites provided by the S/Mo atoms, 2D MoS_2 nanomaterial can be utilized to modify the physicochemical properties of TFC RO membrane surface, including hydrophilicity, roughness and electrostatic charge, which are major factors influencing the membrane permeability and fouling resistance [23].

In this work, a high-performance MoS_2-TFN membrane was fabricated using MoS_2 nanosheets as nanofillers. Few-layered MoS_2 nanosheets were synthesized in high-throughput through liquid exfoliation and characterized systematically. An in depth characterization was carried out to understand the influence of 2 D MoS_2 nanosheets on the physicochemical properties of the resulting TFN membrane, and interfacial interactions. Stability tests were also performed to evaluate the loss of MoS_2 nanosheets from the TFN membrane. The desalination performance of the newly developed MoS_2-TFN membrane was examined in terms of separation and antifouling behavior.

2. Experiments

2.1. Materials and reagents

Polysulfone (PSf) ultrafiltration (UF) membranes with nonwoven polyester fabric were fabricated in the lab through phase inversion (pure water flux at 1.0 bar: 260–270 L m^{-2} h^{-1}, BSA rejection: 96.8%). M-phenylenediamine (MPD, 99%, Sigma-Aldrich) and trimesoyl chloride (TMC, 98%, Sigma- Aldrich) were used as the monomers to establish the active polyamide layer of RO membranes. Furthermore, triethylamine (TEA, 99.5+ %, Sigma-Aldrich), (+)-10-camphorsulfonic acid (CSA, 99%, Sigma-Aldrich) were introduced into the aqueous phase to adjust the pH and catalyze the interfacial polymerization. Isopar G® (ExxonMobil Chemical) was used as solvent to dissolve TMC. The molybdenum disulfide (MoS_2, < 2 μm, 99.5%) was purchased from Sigma Aladin. *N*-Methyl pyrrolidone (NMP, AR, Sinopharm Chemical Reagent Co., Ltd) was selected as the solvent in the exfoliation of MoS_2. Bovine serum albumin (BSA, Sigma-Aldrich) was used as the model foulant in the fouling experiments. The membrane permeability and rejection performance were tested using sodium chloride (NaCl, > 99.7%, Sinopharm Chemical Reagent Co., Ltd).

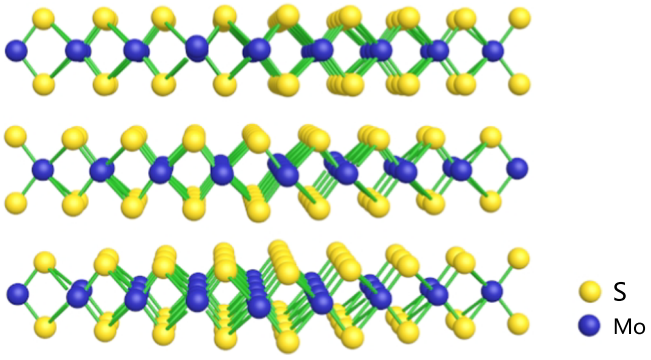

Fig. 1. Illustration of laminar MoS_2 structure.

Deionized (DI) water was used throughout the experiments.

2.2. Preparation of MoS_2 nanosheets

Layered MoS_2 nanosheets were prepared from commercial MoS_2 flakes via solvent assisted liquid exfoliation. In brief, 0.5 g of commercial MoS_2 flakes were immersed into 100 ml NMP solvent in a beaker with capacity of 100 ml. The mixtures were exfoliated for 72 h using a 10 mm diameter probe sonic tip (XO-SM50, 900 W and 25 kHz). To avoid overheating of the probe-tip, the beaker was placed in cold water with an ice bag during the operation. It is necessary to supplement the solvent in a long-time exfoliation due to the solvent evaporation. The resultant brown dispersions were centrifuged at 2000 rpm for 20 min. The suspensions were collected and filtrated through solvent resistant PTFE membrane with pore size of 0.22 μm, following by rinsing the deposits with DI water for several times to removal residue NMP solvent. Finally, the exfoliated MoS_2 nanosheets were dried in an oven at 60 °C. Fig. 1 (S1) illustrates the preparation process of MoS_2 nanosheets.

2.3. Characterization of prepared MoS_2

The morphology of the MoS_2 was observed by transmission electron microscopy (TEM, H-7650, Hitachi, Japan) at an accelerating voltage of 100 kV and atomic force microscopy (AFM, Dimension Icon, Bruker) in tapping mode, respectively. For TEM characterization, the samples were prepared by depositing a drop of 0.01 mg ml^{-1} dispersions of MoS_2 in DI water on the copper grid and dried in a vacuum oven at 60 °C for 48 h. For AFM observation, the sample of MoS_2 dispersion was diluted and dropped on Si substrate, drying at room temperature. The X-ray diffraction (XRD, X'Pert PRO) characterization of MoS_2 nanosheets was carried out with an X-ray diffractometer with Cu Kα radiation (λ = 0.154 nm, D/max-rB 12 kW Rigaku) operated at 40 mA and 40 kV. Absorption spectra of diluted MoS_2 dispersions in NMP were obtained using UV–vis (UV-2450, Shimadzu). The zeta potential of MoS_2 was measured using a Zetasizer 3000HSA (Malvern Instrument) by dispersing the MoS_2 nanosheets in DI water with a concentration of 0.3 mg ml^{-1} at different pH values. Raman spectroscopy was performed on LabRAM Aramis (HORIBA JobinYvon).

2.4. Fabrication of TFC and MoS_2-TFN RO membranes

The TFC and MoS_2-TFN membranes were fabricated via interfacial polymerization on the lab-made PSf support as previously reported [24]. The PSf substrate was cut and taped onto the epoxy resin frame with inner cavity of 19 cm × 13 cm and then immersed in DI water to remove the $NaHSO_3$ before use. The excess water on the PSf substrate layer was removed by drying at room temperature for 3 min and soaked immediately in the amine solution containing 2 wt% MPD and 5.2 wt% TEA-CSA in DI water for 1 min. After draining off the amine solution, tissue paper was employed to gently absorb the excess droplets on the PSf substrate surface, which was then dried for a total of 3 min at room temperature. The prepared PSf membrane was immersed in Isopar G® organic solvent containing 0.1 wt/v % TMC to form a PA layer. The organic solution was poured off after 60 s interfacial polymerization and further kept vertically for another 50 s. Finally, the resultant membrane was dried in an air-circulating oven at 90 °C for 6 min and stored in DI water before testing. The MoS_2-TFN membrane was prepared following the same procedure except that a certain amount of MoS_2 nanosheets (0.005, 0.01, 0.02, 0.05) were dispersed in the organic solution by sonication for 20 min.

2.5. Characterization of TFC and MoS_2-TFN RO membranes

All the prepared membranes were rinsed and dried for 24 h in an oven at 60 °C before being characterized. The observation of the membrane surface and cross-sectional morphologies was carried out using a field-emission scanning electron microscope (FE-SEM, HITACHI S-4800) equipped with an X-ray energy dispersive spectroscope (EDS). Transmission electron microscopy (TEM) was performed with H-7650, Hitachi, Japan operating at 100 kV accelerating voltage to study the morphologies of thin film cross-section of TFC membrane and TFN membranes. Small pieces of the fabric free membrane samples were embedded in Epon resin and cut by an ultramicrotome. The contact angles were measured with a 3.0 μL DI water drop using the sessile drop method on a video contact angle system (OCA20, Dataphysics, German). The average value of five measurements at random positions for each sample was reported. The surface roughness of prepared membranes was measured by AFM (Dimension Icon, Bruker) with tapping mode measurements in air. The root mean square roughness (R_q), root average arithmetic roughness (R_a) and the mean difference between the highest peaks and lowest valleys (R_{max}) were used to analyze the membrane surface roughness for a scanning area of 5 μm × 5 μm for each sample. The chemical compositions of the PA top surfaces were analyzed by X-ray Photoelectron Spectroscopy (XPS) (ESCALAB 250Xi, Thermo Fisher) using an Al Kα radiation as X-ray source. Survey spectra and the narrow scan spectra of Mo 3d and S 2p peaks were collected. Raman spectra of membranes were obtained using LabRAM Aramis (HORIBA JobinYvon). The membrane samples were cut into 1.0 cm × 1.0 cm before characterization. Excitation was provided by a 632.8 nm He-Ne laser. A 50 × objective (Olympus) was used to focus the laser beam and collect the Raman signal.

2.6. Evaluation of desalination performance

The desalination performance of the prepared RO membranes was evaluated using a stainless-steel cross-flow membrane module (Sterlitech) with effective testing membrane area of 42 cm^2. The separation equipment was operated at a flow rate of 60 L h^{-1} under 15.5 bar and the temperature was maintained at 25 °C controlled by the water cooling system. The feed was prepared with 2000 ppm NaCl solution with osmotic pressure of 1.69 bar in a tank of 10 L. The water flux (J_w) and apparent salt rejection (R_{NaCl}) were calculated from the following equations:

$$J_w = Q/(A \times t)$$

where J_w (L m^{-2} h^{-1}) is the water flux, Q (L) is the volume of permeate water during a time interval t (h), and A (m^2) is the effective area of the testing membrane:

$$R_{NaCl} = (1 - C_p/C_f) \times 100\%$$

$$R(\%) = \left(1 - \frac{c_p}{c_f}\right) \times 100$$

where c_pC_p and C_f $c_f$are the salt concentration in the permeate and feed solutions, respectively. The salt concentration was determined by a portable conductivity meter (sensION + EC5, HACH).

2.7. Stability test of TFN membrane

To evaluate the long-term stability of TFN membrane, the prepared 0.01 wt% MoS_2-TFN membrane was tested with 2000 ppm NaCl solution at a pressure of 15.5 bar for 20 h continuously. Permeates and the feed cycling water (3 L) were collected for the analysis of MoS_2 loss, using UV–vis. The MoS_2 concentration as a function of the optical absorbance was achieved by dispersing MoS_2 nanosheets in 2000 ppm NaCl solution with known concentration (0, 0.4, 1.0, 2.0, 10, 20 mg/L); the absorbance was measured at a wavelength of 674 nm (the maximum absorbance wavelength) after the background subtraction. The concentration of MoS_2 in the permeate water and in the cycling water was estimated based on the Lambert-Beer law, A/l = αC, where A/l represents the absorbance per cell length, α was obtained from the

slope of the curve. XPS was further utilized to investigate the binding energy MoS_2 on TFN membrane before and after filtration.

2.8. Evaluation of membrane antifouling properties

Membrane antifouling properties were evaluated by filtration experiments with an aqueous solution and a model foulant. Prior to the fouling test, the membranes were compacted under 2000 ppm NaCl solution at pressure of 15.5 bar for 3 h to achieve flux and salt rejection in steady state condition. The fouling test was performed immediately using 2000 ppm NaCl feed solution containing 100 ppm bovine serum albumin (BSA) as a model protein foulant at 15.5 bar, 25 °C. The normalized water flux J_n was obtained by the following equation:

$$J_n = J_f/J_0$$

where J_f is the instantaneous water flux varied with time in the filtration process and J_0 is the initial water flux. The desalination and antifouling performance of the commercial brackish water desalination membrane BW-30 was evaluated in this work following identical procedures.

3. Results and discussion

3.1. Physicochemical characterization of laminar MoS_2

NMP was used as the dispersion/exfoliation solvent because of the matching solubility parameters of solvent and MoS_2 [25]. Several characterization techniques were used to understand the physicochemical properties of prepared layered MoS_2. The morphology of prepared MoS_2 was investigated by TEM and AFM. As can be seen in Fig. 2 a, the prepared MoS_2 exhibited two-dimensional irregular shapes with a well-defined layered structure. The ultrathin graphene-like morphology was without any wrinkles, and was stacked uniformly. The comparison between bulk MoS_2 crystals and the prepared layered MoS_2 nanosheets shown in Fig. S2 suggests that the dimensions of MoS_2 nanosheets could be reduced effectively with exfoliation time. The AFM image shown in Fig. 2 b reveals that the lateral size of 72 h exfoliated MoS_2 nanosheets was between 100 and 600 nm (except few larger flakes in size of micrometers) with a high density of pore defects on the surface. These structure defects were confirmed by the sharp in-depth in the height profile at the distance of 1.3 μm in Fig. 2c, which was mainly attributed to the intensive exfoliation energy input. The thickness of the exfoliated layered MoS_2 was measured to be ca. 2.2 nm, as shown in Fig. 2c. Considering the thickness of a single layer and the lateral gap of layered MoS_2 was reported to be ~0.62 nm [26,27], the number of nanosheets was estimated to be within 3 layers. It was believed that there were also exfoliated single layer MoS_2 nanosheets in the products (Inset TEM image in Fig. 2a). Recently, IPA/water mixtures were found suitable as a more benign solvent to obtain functionalizable mono- and few-layered MoS_2 nanosheets (1–10 layers) by exfoliating the MoS_2 crystals due to the matched surface tension components [28–30]. However, the exfoliated nanosheets may reaggregate if the matched surface tension is changed [30]. The good balance could be varied due to the evaporation of water during the long-term and high energy input exfoliation process. Besides, the concentration of exfoliated MoS_2 nanosheets was typically lower by a factor of three compared to NMP [29]. Therefore, NMP was preferentially chosen as exfoliation solvent in this work by considering the high efficiency and ease of preparation.

The optical absorption of a series of MoS_2 dispersions in *N*-methyl-2-pyrrolidone (NMP) at different exfoliation times was measured. As shown in Fig. 3 a, the excitation peaks at 614 nm and 674 nm are the typical absorbance of two dimensional MoS_2 [31,32]. The variation of the scattering exponent (the slope of the dashed line in Fig. 3 a) with different exfoliation times indicates the decreasing MoS_2 lateral size. After subtracting the scattering background, the typical spectrum of MoS_2 was obtained (Fig.3a inset). Fig. 3 b shows typical Raman spectra for prepared laminar MoS_2 before and after 72 h liquid exfoliation. The laminar MoS_2 exhibits two Raman characteristic bands at ~404 and 386 cm^{-1}, ascribed to the A_{1g} and E_{2g} modes, respectively [22,27]. To explore the crystalline structure of exfoliated MoS_2 nanosheets, XRD was used (shown in Fig. 3 c). The strong peak at $2\theta = 14.4^\circ$ corresponds to the (002) basal plane of MoS_2, and the basal spacing can be calculated as 0.62 nm according to Bragg's law, which is in agreement with the literature [22]. The zeta potential represents a useful qualitative probe to verify the abundance of sulphur edge sites on the prepared laminar MoS_2. The results shown in Fig. 3 d demonstrate that MoS_2 is highly negatively charged when dispersed in water at various pH values. More negative zeta potentials over the pH range 2 to 12 for MoS_2 nanosheets than MoS_2 bulk crystal infer the presence of more MoS_2 sulphur edge sites on the nanosheets, in agreement with the observations made in the SEM image in Fig. S3. At neutral pH, the zeta potential of the liquid exfoliated laminar MoS_2 was measured −30.4 mV.

3.2. Characterization of TFC and TFN membranes

The surface and cross-section morphologies of TFC and TFN membranes were observed using SEM. The surface morphologies of the TFN membranes changed with addition of MoS_2 nanosheets, are shown in Fig. 4. When the MoS_2 content reached 0.01 wt% (Fig. 4b and c), surface features of the membrane appeared to be less leaf-like and have more small nodular structures compared with the surface of TFC

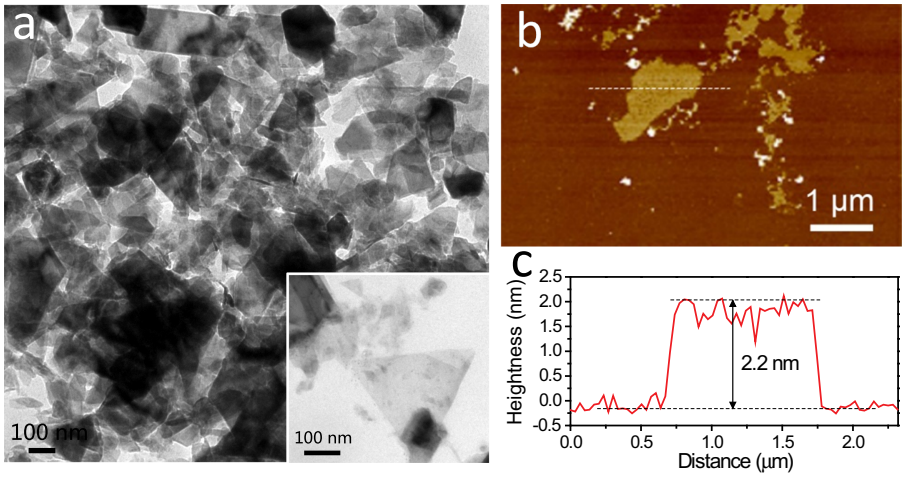

Fig. 2. Surface morphology characterization of prepared laminar MoS_2, (a) TEM image, (b) AFM image and (c) height profile.

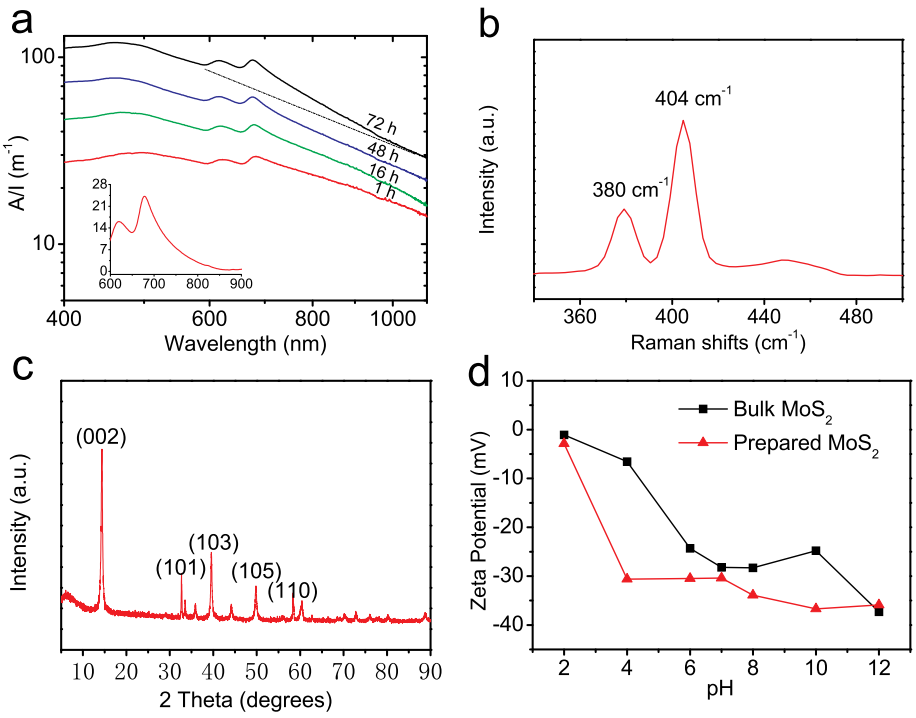

Fig. 3. (a) UV–vis absorbance spectra of MoS_2 dispersions in NMP prepared with different exfoliation time. Inset: The spectrum of the 72 h exfoliated dispersions after subtraction of scattering background (dashed line in main figure). (b), (c) Raman shifts and XRD pattern of prepared MoS_2, respectively. (d) Zeta-potential of as-prepared MoS_2 dispersed in water with different pH values.

membrane (Fig. 4a). This could also be seen in Fig. 5. Generally, the aromatic polyamide TFC membrane is formed by interfacial polymerization through MPD diffusing from the aqueous phase into the organic phase to react with TMC. The two dimensional MoS_2 nanosheets in the organic phase reduced the reaction zone by limiting the MPD diffusion and penetrating into the depth of the organic phase, which may result in a change in surface morphology. The white circle in Fig. 4b is believed to be MoS_2 nanosheets because of their two dimensional shape, which is consistent with the size of prepared MoS_2 (Fig. 2). These MoS_2 nanosheets were visible on all TFN membranes surfaces in Fig. 4b-e. At low MoS_2 loading, the nanosheets distributed randomly on the PA film. However, at higher MoS_2 loading (Fig. 4d and e), particularly Fig. 4e, the MoS_2 nanosheets aggregate and cover the PA surface. The agglomeration was mainly caused by the strong surface energy of inorganic MoS_2 nanosheets in the non-polar organic solvent. The cross-section SEM images of TFC membrane and 0.01 wt% MoS_2-TFN membrane were shown in Fig. S4a and S4b, respectively. The 2 D MoS_2 nanosheets could be easily found in the membrane PA matrix (Fig. S4b).

Since the incorporated inorganic fillers exhibited an easily discerned dark and specific shape under the electron beam, TEM is considered to be a convincible technique to provide the dispersion information of nanomaterials within the PA thin film layer. As shown in Fig. 5 a and 5 b, a leaf-like structure was observed for the TFC membrane. This is the typical membrane formed through interfacial polymerization between MPD in the aqueous phase and TMC in Isopar G® organic phase [24,33]. The PA thickness is ~272 nm. In Fig. 5c, the MoS_2 nanosheets with their distinct 2 D rectangular structure appeared darker than the polymer and were clearly observed embedded under a continuous PA skin layer in the polysulfone side for 0.01 wt% MoS_2-TFN membrane. It was also observed that a large quantity of MoS_2 nanosheets with a size of hundreds of nanometers were distributed within the cross-section of the PA skin layer and covered on the membrane surface (Fig. 5d). This was in accordance with the results shown in Fig. 4. and Fig. 7. It is also found that smaller size of MoS_2 nanosheets were well distributed in PA matrix, which is shown in Fig. S5. The thickness of the selective layer for 0.01 wt% MoS_2-TFN membrane is ~179 nm (Fig. 5d), which is significantly lower than that of the TFC membrane. The TEM for the

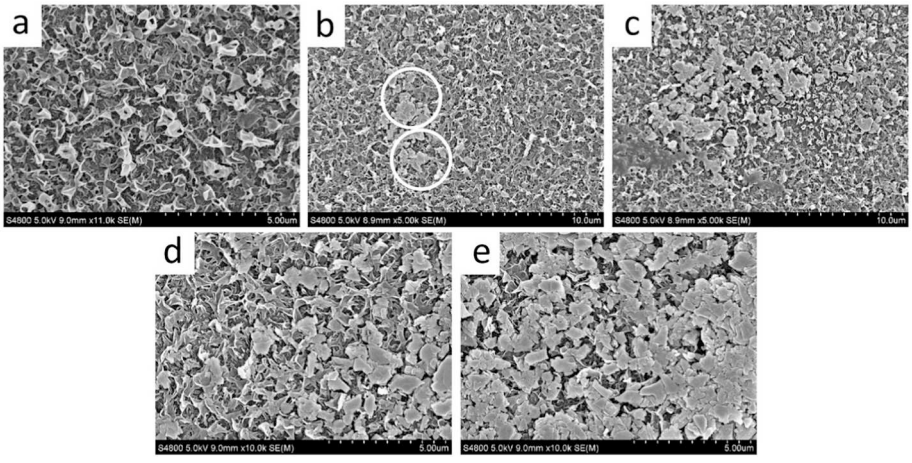

Fig. 4. SEM images of (a) TFC membrane, (b) 0.005 wt% MoS_2-TFN, (c) 0.01 wt% MoS_2-TFN, (d) 0.02 wt% MoS_2-TFN and (e) 0.05 wt% MoS_2-TFN membranes.

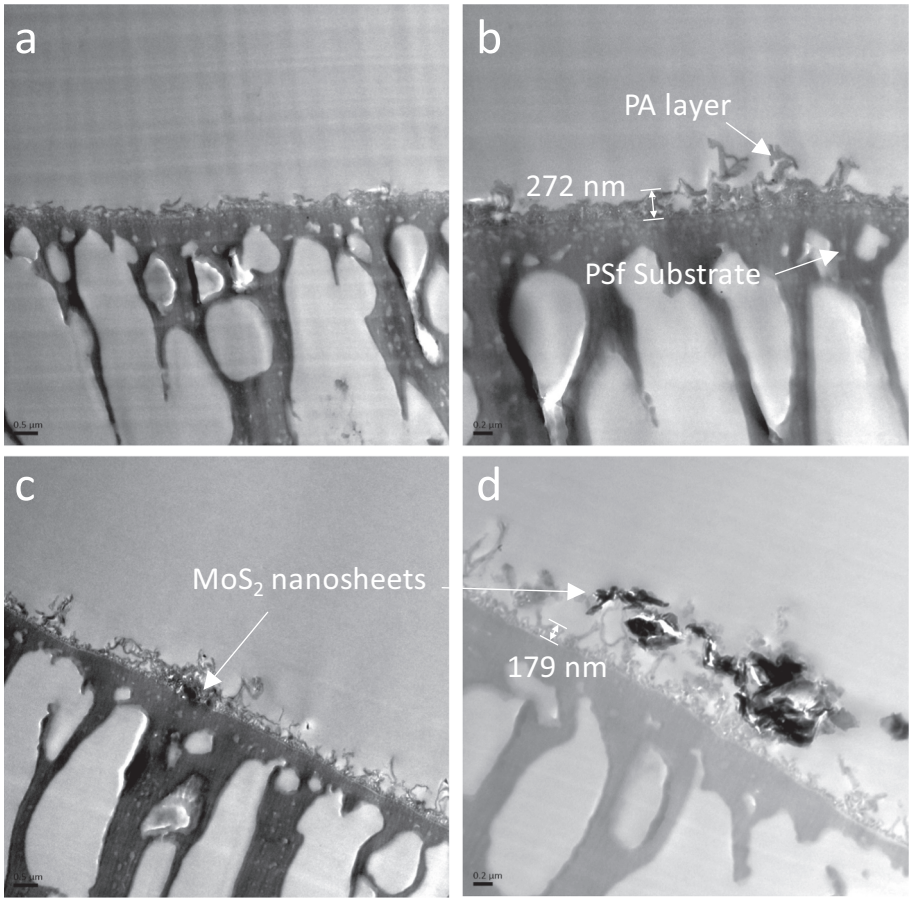

Fig. 5. TEM images for the cross-section of TFC membrane (a, b) and 0.01 wt% MoS_2-TFN membrane (c, d). (a, c: under 10,000× magnification and b, d under 20,000× magnification).

cross-section characterization of the TFN membrane confirmed the incorporated MoS_2 nanosheets are not only present on the membrane surface but also distributed within the dense thin film layer, which demonstrates the successful modification of TFN membranes using 2 D MoS_2 nanosheets. SEM/EDS elemental mapping allowed further analysis of the distribution of elements and revealed the distribution of MoS_2 nanosheets on the membrane surface (Fig. S6).

The membrane surface morphology and roughness parameters of TFC and TFN membranes were investigated using AFM measurement. Three-dimensional scan images (5 μm × 5 μm) are displayed in Fig. 6. It can be observed that the addition of MoS_2 nanosheets in the organic phase of a TFN membrane creates a rougher surface. A more expressed

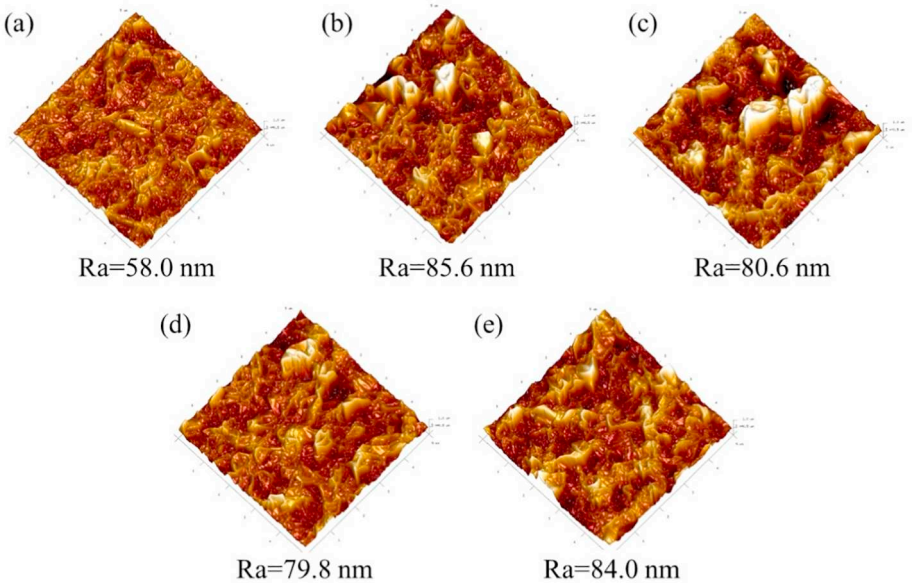

Fig. 6. AFM images for TFC (a) and TFN membranes (b–e).

"ridge-and-valley" PA morphology was observed for TFN membranes compared to the TFC membrane (Fig. 6(a)). Table 1 summarizes the surface roughness parameters R_a, R_q and R_{max} on nanoscopic scale. All three values increased substantially for TFN membranes. With increasing the MoS_2 loading, the R_{max} value reduced gradually because the stacked two dimensional nanosheets decreased the PA leaf structure, which in agreement with the SEM images (Fig. 4 (e)). The rougher membrane surfaces were expected to provide effective higher surface area for water permeation.

The EDS results of TFC and TFN membranes in Table S1 highlight the increasing Mo element in TFN membranes compared with the unmodified TFC membrane. However, due to the overlapping orbital energy between S and Mo, the EDS result was not convincing enough to provide evidence for the presence of MoS_2 in the TFN membranes. XPS was applied to reveal the chemical composition of each membrane. The wide scan XPS spectra of TFC and TFN membrane were investigated and shown in Fig. 7 (a). There were three major peaks at 284.1 eV, 531 eV and 399.2 eV that could be ascribed to the binding energies of C 1 s, O 1 s and N 1 s, respectively [34,35]. Two new peaks appeared, corresponding to the Mo 3d and S 2p. Fig. 7 (b) shows two peaks at 228.9 eV and 231.7 eV, which can be attributed to the doublet of Mo 3 $d_{5/2}$ and Mo 3 $d_{3/2}$ [36]. The binding energy for S 2 $p_{3/2}$ and S 2 $p_{1/2}$ is 161.5 eV and 162.7 eV [27], shown in Fig. 7 (c). The Mo and S binding energies indicate that layered MoS_2 nanosheets successfully modified the PA film and are chemically stable.

Raman spectroscopy was further utilized to analyze the distribution of layered MoS_2 nanosheets in the PA bulk matrix. Two areas for a TFN membrane with (area B marked in blue) and without (area A marked in red) coverage of layered MoS_2 nanosheets were detected. The results are shown in Fig. 7(d). The spectrum of the TFC membrane clearly shows symmetric C—O—C stretching (~1147 cm^{-1}) and phenyl ring vibration (~1590–1620 cm^{-1}) [37]. Compared with the spectrum of area A, the intensity of the peaks of 1147 cm^{-1} and 1620 cm^{-1} was decreased while the typical Raman peaks of MoS_2 were observed at 380 cm^{-1} and 406 cm^{-1}, which indicates that the MoS_2 nanosheets were embedded into the PA matrix. However, in area B, the spectrum has a close similarity with pure MoS_2 Raman shifts, which gave direct evidence for the observed MoS_2 objects in SEM Fig. 4 (b). It demonstrated that the incorporated inorganic MoS_2 nanosheets distributed in the interlayer between the PSf substrate and the top region of the PA film are in accordance with the TFN membranes prepared with fillers incorporated in the organic phase reported elsewhere [38–41].

Fig. 8 shows that the contact angle of the TFN membrane with 0.01 wt% MoS_2 loading in the organic phase decreases to 71°, which indicates an improved membrane surface hydrophilicity. With further increasing MoS_2 concentration, the contact angle of the TFN membranes increases. However, because of the inferior hydrophilicity of MoS_2 nanosheets compared to PA polymer, the surface distributed MoS_2 nanosheets as observed in Fig. 4(d, e) at higher loading content have a decreasing effect on the water contact angle, so that the hydrophilicity of membrane surfaces is reduced. This was similar to the results observed when the hydrophobic ZIF-8 in the organic phase was incorporated into the PA layer [38].

3.3. Separation performances of TFC and TFN membranes

Fig. 9 shows the effect of MoS_2 loading on water flux and salt rejection of TFN membranes. Compared with a pristine TFC membrane, the water flux of PA TFN membranes showed a significant increase when the MoS_2 loading content increased to 0.01 wt%, and then decreased slightly with further increasing MoS_2 concentration. At 0.01 wt % MoS_2 loading in the organic phase, the TFN membrane was found to have the water flux, i.e., 92.9 L m^{-2} h^{-1} (6.2 L m^{-2} h^{-1} bar^{-1}), which was 1.2 times higher than that of a pristine TFC membrane (78.6 L m^{-2} h^{-1}). At the same time, the salt rejection of all MoS_2 modified TFN membranes was higher than that of the TFC membrane. In general, a high content of filler incorporation leads to a loss of salt rejection due to the defects or voids caused by the aggregation of fillers in the selective polyamide skin layer. Nevertheless, a higher loading of MoS_2 nanosheets led to a better salt rejection, with 99.2% for 0.05 wt% content of MoS_2 incorporated TFN membrane compared to 98.1% for the TFC membrane. Thus, the MoS_2 nanosheets play a dominant role in the selectivity improvement for TFN membranes. Overall, the 0.01 wt% MoS_2-TFN membrane showed the optimum separation performance in consideration of both the water flux and salt rejection.

The remarkable enhancement of separation performance was primarily attributed to the decreased selective skin layer thickness and the increase of membrane surface roughness as well as the enhanced surface hydrophilicity, as observed in Fig. 5, Fig. 6 and Fig. 8, respectively. In addition, the hydrophilic sites of laminar MoS_2 nanosheets gave rise to a high affinity to water molecules through hydrogen bonding, which leads to the increased water flux [12]. Furthermore, the negatively charged MoS_2 nanosheets could construct barriers for salt ions through sieving effect and electrostatic repulsion interactions in the PA TFN membrane matrix. A scheme for the TFN membrane fabrication process and the mechanism leading to the superior desalination performance is proposed in Fig. 10. The nonselective voids caused by the inferior compatibility of inorganic and polymer matrix could also contribute to the enhanced water permeability [42]. However, the hindrance of lamellar MoS_2 for water transportation in membrane by creating a more tortuous pathway for water molecules should not be overlooked. At higher MoS_2 loading content in the organic phase, the impermeable inorganic MoS_2 agglomerations would cause a reduced water flux.

3.4. Evaluation of membrane antifouling performance

Bovine serum albumin (BSA), a negatively charged biopolymer, was selected as the model protein foulant in the membrane fouling test. The variation of normalized water flux and apparent salt rejection in the presence of 100 ppm BSA and 2000 ppm NaCl is presented in Fig. 11. In the initial 3 h, both the TFC and TFN membranes showed a decline in water flux, down to 90%, 95% of its initial water flux, respectively (Fig. 11(a)). After 14 h filtration, the normalized water flux of the TFC membrane reduced to 86% while the MoS_2 modified TFN membrane exhibited a relatively unapparent decline of the normalized water flux to around 91%, indicating an enhanced fouling resistance. Meanwhile, the apparent NaCl rejection of both TFC and TFN membrane increased sharply when BSA was present in the feed (Fig. 11(b)). The TFN membrane maintained a better salt rejection, of over 99.2% compared with the rejection of the TFC membrane, which was 98.9%.

To explore the TFN membrane anitifouling behavior, the surface morphology of a TFN membane and the TFC membrane after 14 h BSA fouling test were investigated by SEM. As shown in Fig. 11(c), the TFC membrane was intensively polluted. BSA particles were aggregated on the membrane surface by interwining with the PA leaf-like structures, resulting in an instantly reduced water flux. In comparison, a TFN membrane (Fig. 11(d)) exhibits a lower coverage of BSA foulants on the membrane surface, suggesting the impoved fouling resistance. The improved antifouling property could be attributed to two main reasons: on the one hand, the incorporated negatively charged nanosheets gave

Table 1
Surface roughness parameters of TFC and TFN membranes.

Membrane	Surface roughness parameters		
	R_a (nm)	R_q (nm)	R_{max} (nm)
TFC	58.0	74.3	595.3
0.005 wt% MoS_2-TFN	85.6	112.3	918.3
0.01 wt% MoS_2-TFN	80.6	101.0	825.5
0.02 wt% MoS_2-TFN	79.8	102.1	758.3
0.05 wt% MoS_2-TFN	84.0	106.5	739.0

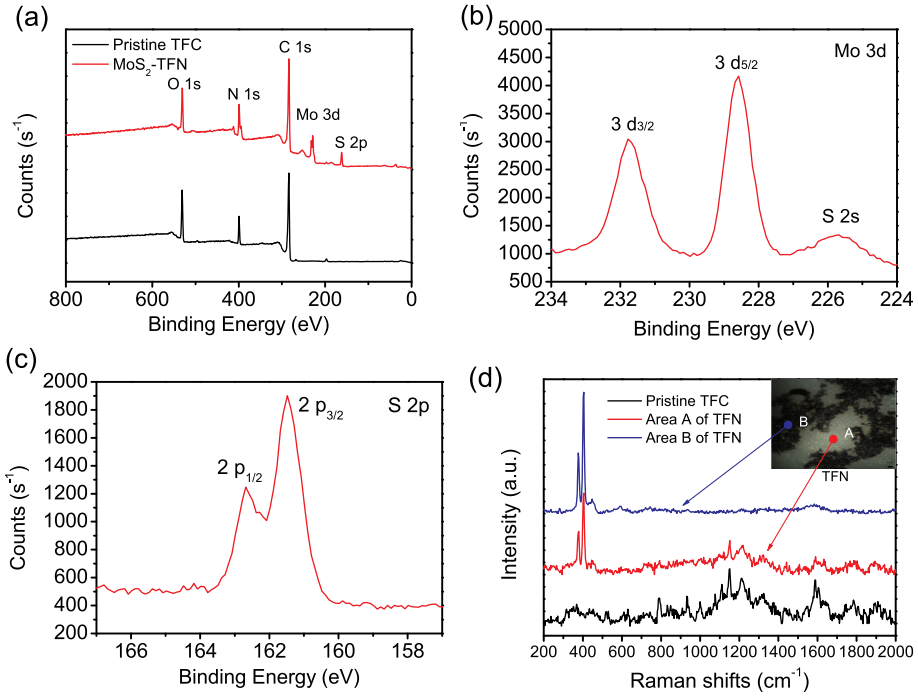

Fig. 7. (a) XPS spectra for pristine TFC and MoS_2-TFN membrane. (b) Mo 3d and (c) S 2p narrow scan XPS spectra for TFN membrane, respectively. (d) Raman spectra of pristine TFC membrane and area A, area B for 0.01 wt% MoS_2-TFN membrane. Inset: 0.01 wt% MoS_2-TFN membrane.

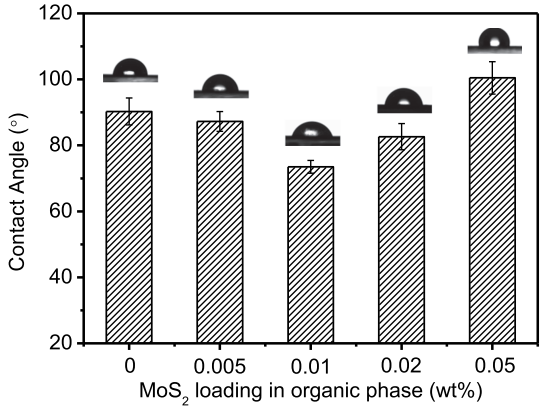

Fig. 8. Water contact angle measurements of TFC and MoS_2-TFN membranes with different loading content.

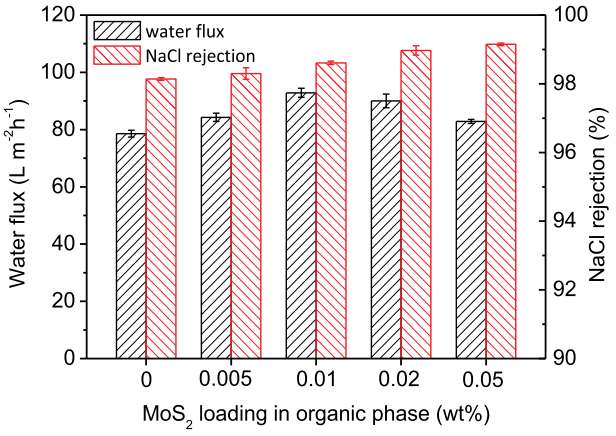

Fig. 9. Water flux and salt rejection of TFC, TFN membranes with different MoS_2 loading (2000 ppm, 15.5 bar, 25 °C).

rise to repulsive interactions between the BSA and TFN membrane surfaces through electricstatic forces [43]. On the other hand, the flat nanosheets on the membrane surface provide less possibility for deposition and attachment of foulants [44]. The possible mechanism is illustrated in Fig. 10. Therefore, the negatively charged nanosheets are believed to effectively enhance the TFN membrane resistance against fouling [45].

3.5. Stability test of MoS_2-TFN membrane

Nanomaterial could pose challenges to the environment, and may entail human health concerns as well. Considering the inferior compatibility of inorganic material in a polymer matrix, it was necessary to evaluate the loss of MoS_2 from the PA layer under dynamic conditions. Therefore, a long term (20 h) filtration experiment was carried out to assess the loss of MoS_2 from the 0.01 wt% MoS_2-TFN membrane. The standard curve inset in Fig. 12 (a) shows that the optical absorbance of MoS_2 after background subtraction scaled linearly with the MoS_2 concentration in water, allowing the estimation of the extinction coefficient to be $\alpha = 2146.44\ L\ g^{-1}\ m^{-1}$. Consequently, the total loss in permeate water and recycling water as a function of operation time was calculated based on Lambert-Beer's law and presented in Fig. 12 (a). The rapid increase of MoS_2 in the recycling water indicates that the 0.01 wt % MoS_2-TFN membrane suffers from a loss in the dynamic process. At the start of 2 h operation, up to 1.5 mg was released from the TFN membrane. However, it remains stable after 6 h in the long term filtration process with total loss of around 1.6 mg. In contrast, MoS_2 was not detected in the permeate water in the entire filtration test, which demonstrates the stability of the MoS_2 nanosheets in the polymer matrix. The wide span XPS spectrum for the TFN membrane before and after filtration is presented in Fig. 12 (b). The binding energy of Mo 3d and S 2p for a TFN membrane after filtration decreases to a large extent. This could be confirmed by the narrow scan spectra of Mo 3d and S 2p in Fig. 12(c) and (d), respectively, compared with that of a TFN membrane before filtration (Fig. 7(b) and (c), respectively). The non-

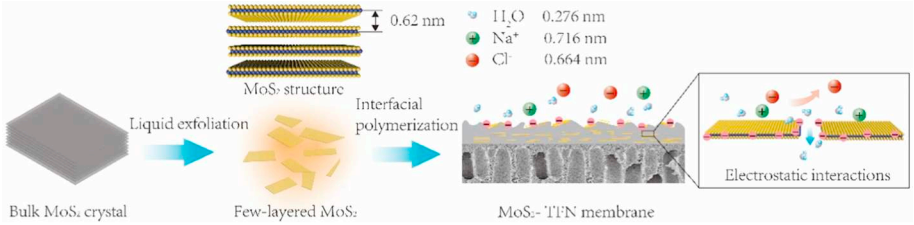

Fig. 10. Scheme of MoS_2-TFN membrane fabrication process and the underlying mechanism for superior desalination performance.

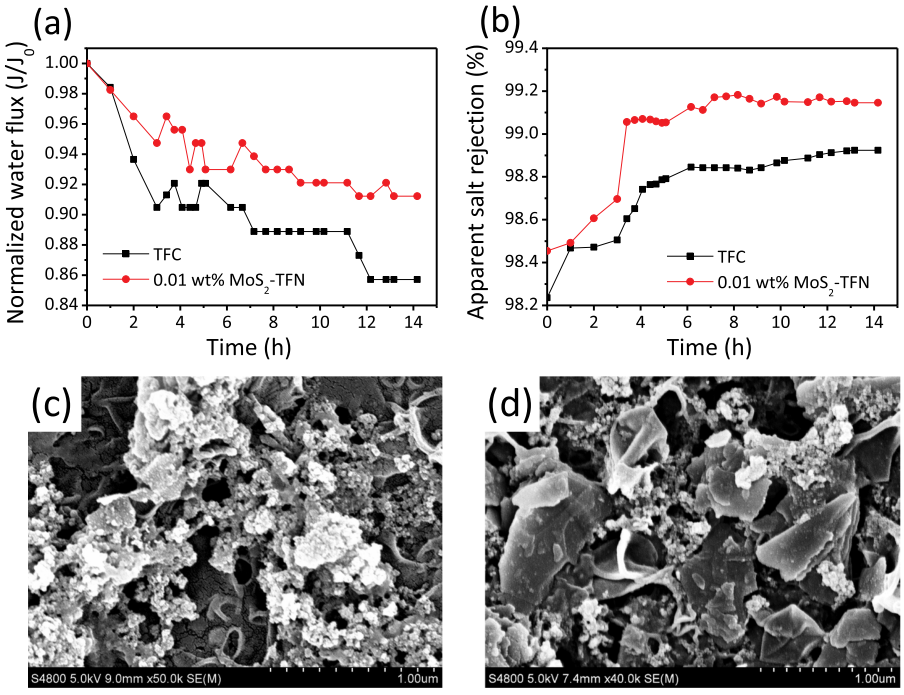

Fig. 11. Variation of normalized water flux (a) and apparent salt rejection (b) with time for TFC membrane and 0.01 wt% MoS_2-TFN membrane. SEM images of surface morphology of TFC membrane (c) and 0.01 wt% MoS_2-TFN membrane (d) after fouling test. Test conditions: BSA 100 ppm, NaCl 2000 ppm, pH 6.8, operation pressure 15.5 bar, temperature 25 °C.

covalent bonding between MoS_2 nanosheets and the PA matrix ensures the stability in the harsh dynamic conditions. It can be concluded that the TFN membrane embedded with MoS_2 nanosheets is suffering a slight loss in the initial operation, and stabilizes with time in the filtration process. In order to investigate the influence of the loss of MoS_2 nanosheets from modified membranes on the water flux and salt rejection, the filtration performance of a 0.01 wt% MoS_2-TFN membrane was measured during 20 h. The results are shown in Fig. S7a. Due to the compaction of the membrane under high pressure, an instant decrease of the water flux was observed and maintained stable after 1 h (Fig. S7b). In contrast, the salt rejection decreased during the first 4 h (Fig. S7c). It is probably caused by the TFN membrane suffering from the loss of MoS_2 nanosheets in the initial 2 h, which reduced the electrostatic repulsion from the membrane surfaces for salt ions. However, this effect was not significant for the membrane stability in the long-term filtration process.

Table 2 compares the performance of a MoS_2-TFN membrane with the state-of-art commericial and lab-made RO membranes measured under the same test conditions. It is clear that the MoS_2-TFN membrane outperformes the BW-30 brackish water desalination RO membrane and most of the lab fabricated TFN RO membranes in terms of water flux and antifouling properties.

4. Conclusions

Few-layered MoS_2 sheets were prepared by liquid-phase exfoliation from bulk MoS_2 crystals and incorporated with different loading content into the TFN membrane PA matrix via interfacial polymerization. It was observed that layered MoS_2 played an important role in membrane surface modification, rendering the TFN membrane with decreased selective layer thickness, improved surface hydrophilicity and surface roughness. The 0.01 wt% MoS_2-TFN membrane showed the optimal water permeability of 6.2 $L\,m^{-2}\,h^{-1}\,bar^{-1}$ and salt rejection of 98.6% using the 2000 ppm NaCl solution at 15.5 bar, 25 °C. Fouling experiments demonstrated that 91% of the normalized water flux was maintained for 0.01 wt% MoS_2-TFN membrane using 100 ppm BSA as the protein foulant, which suggests the improved antifouling properties. The high water-salt selective and superior fouling resistant MoS_2-TFN RO membrane outperforms the state-of-the-art commercial RO membranes and many of the hand cast TFN membranes. Future work needs to focus on addressing the dispersion of MoS_2 in the membrane matrix as well as the loss of MoS_2 nanosheets in the retentate. The in-situ modification of a TFC-PA RO membrane using 2D nanomaterial as filler was found promising to produce high perm-selectivity and fouling resistant TFN RO membranes.

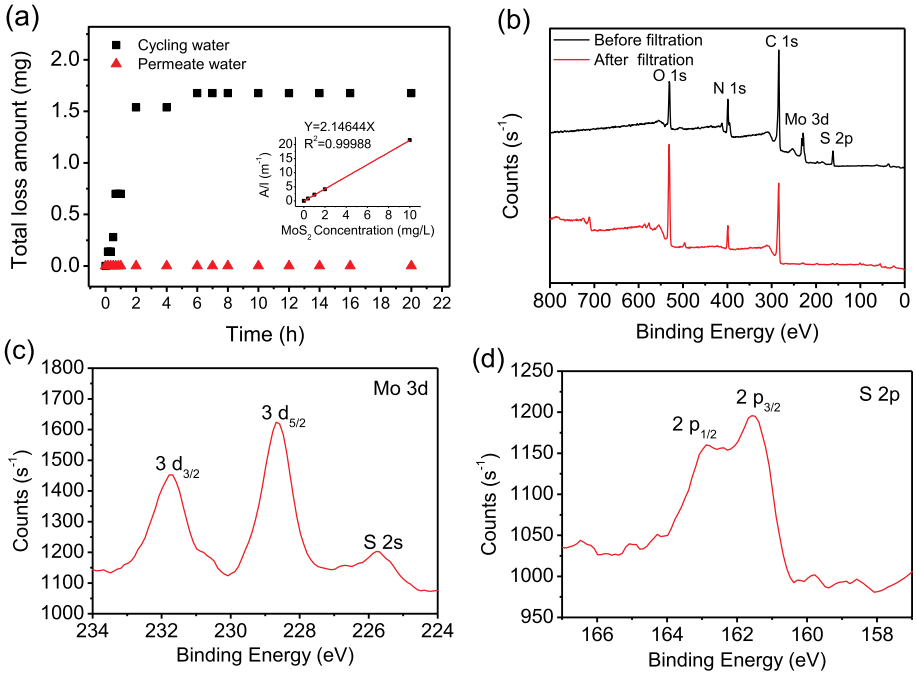

Fig. 12. Total loss amount of MoS_2 on modified TFN membrane with time during operation (3 L volume of 2000 ppm NaCl feed solution as cycling water). (inset: absorbance of different concentration of MoS_2 dispersed in DI water under 674 nm wavelength).

Table 2
Desalination performance of commercial RO membrane, TFC membrane and MoS_2- TFN membranes.

Membranes	2000 ppm NaCl		NaCl and protein foulant		Ref.
	Flux ($L\,m^{-2}\,h^{-1}$)	R_{NaCl}[a] (%)	Flux ($L\,m^{-2}\,h^{-1}$)	Normalized flux (J_n)	
BW-30	62.9	98.3	54.7	0.87	This work
TFC	78.6	98.1	67.4	0.86	This work
MoS_2-TFN	92.9	98.6	84.5	0.91	This work
MMT-TFN[b]	51.7	99	40.8	0.79	[9]
LDH-TFN[b]	41.7	99.3	29.2	0.70	[9]
rGO/TiO_2 - TFN[c]	51.3	99.45	38.5	0.75	[46]
GO_{10}-coated PA	14.0	96.4	11.9	0.85	[47]

[a] R_{NaCl}: apparent salt rejection.
[b] Test conditions: using protein foulant BSA 60 ppm and 2000 ppm NaCl; DTAB 25 ppm, 2000 ppm NaCl, at pressure 16 bar.
[c] Test conditions: BSA 500 ppm for 3 h.

Acknowledgements

This work was financially supported by the Key Project of International Cooperation, Bureau of International Cooperation, Chinese Academy of Sciences (132C35KYSB20160018) and the Key Project of Frontier Science, CAS. The authors acknowledge Youming Rong, Xin Wu and Huali Tian for their assistance in laminar MoS_2 preparation. The authors also thank Hongyun Ren at the Center of Analysis & Measurement from Institute of Urban Environment, Chinese Academy of Sciences for the TEM measurement.

Appendix A. Supplementary data

Supplementary data to this article can be found online at https://doi.org/10.1016/j.desal.2018.12.016.

References

[1] M. Elimelech, W.A. Phillip, The future of seawater desalination: energy, technology, and the environment, Science 333 (2011) 712–717.
[2] S.Y. Lee, H.J. Kim, R. Patel, S.J. Im, J.H. Kim, B.R. Min, Silver nanoparticles immobilized on thin film composite polyamide membrane: characterization, nanofiltration, antifouling properties, Polym. Adv. Technol. 18 (2007) 562–568.
[3] J.R. Werber, C.O. Osuji, M. Elimelech, Materials for next-generation desalination and water purification membranes, Nat. Rev. Mater. 1 (2016) 16018.
[4] R.K. Joshi, P. Carbone, F.C. Wang, V.G. Kravets, Y. Su, I.V. Grigorieva, H.A. Wu, A.K. Geim, R.R. Nair, Precise and ultrafast molecular sieving through graphene oxide membranes, Science 343 (2014) 752–754.
[5] J. Wang, P. Zhang, B. Liang, Y. Liu, T. Xu, L. Wang, B. Cao, K. Pan, Graphene oxide as an effective barrier on a porous nanofibrous membrane for water treatment, ACS Appl. Mater. Interfaces 8 (2016) 6211–6218.
[6] Y. Han, Z. Xu, C. Gao, Ultrathin graphene nanofiltration membrane for water purification, Adv. Funct. Mater. 23 (2013) 3693–3700.
[7] J. Lee, J.H. Jang, H.-R. Chae, S.H. Lee, C.-H. Lee, P.-K. Park, Y.-J. Won, I.-C. Kim, A facile route to enhance the water flux of a thin-film composite reverse osmosis membrane: incorporating thickness-controlled graphene oxide into a highly porous support layer, J. Mater. Chem. A 3 (2015) 22053–22060.
[8] Q. Liu, G.-R. Xu, Graphene oxide (GO) as functional material in tailoring polyamide thin film composite (PA-TFC) reverse osmosis (RO) membranes, Desalination 394 (2016) 162–175.
[9] H. Dong, L. Wu, L. Zhang, H. Chen, C. Gao, Clay nanosheets as charged filler materials for high-performance and fouling-resistant thin film nanocomposite membranes, J. Membr. Sci. 494 (2015) 92–103.
[10] S. Dervin, D.D. Dionysiou, S.C. Pillai, 2D nanostructures for water purification: graphene and beyond, Nanoscale 8 (2016) 15115–15131.
[11] J. Lawler, Incorporation of graphene-related carbon nanosheets in membrane fabrication for water treatment: a review, Membranes (Basel, Switz.) 6 (2016).
[12] L. Sun, H. Huang, X. Peng, Laminar MoS2 membranes for molecule separation, Chem. Commun. (Camb.) 49 (2013) 10718–10720.
[13] J. Feng, M. Graf, K. Liu, D. Ovchinnikov, D. Dumcenco, M. Heiranian, V. Nandigana, N.R. Aluru, A. Kis, A. Radenovic, Single-layer MoS2 nanopores as nanopower generators, Nature 536 (2016) 197–200.
[14] M. Heiranian, A.B. Farimani, N.R. Aluru, Water desalination with a single-layer MoS2 nanopore, Nat. Commun. 6 (2015) 8616.
[15] L. Sun, Y. Ying, H. Huang, Z. Song, Y. Mao, Z. Xu, X. Peng, Ultrafast molecule separation through layered WS(2) nanosheet membranes, ACS Nano 8 (2014) 6304–6311.
[16] S. Qin, D. Liu, G. Wang, D. Portehault, C.J. Garvey, Y. Gogotsi, W. Lei, Y. Chen, High and stable ionic conductivity in 2D nanofluidic ion channels between boron nitride layers, J. Am. Chem. Soc. 139 (2017) 6314–6320.
[17] W. Lei, D. Portehault, D. Liu, S. Qin, Y. Chen, Porous boron nitride nanosheets for effective water cleaning, Nat. Commun. 4 (2013) 1777.
[18] C.E. Ren, K.B. Hatzell, M. Alhabeb, Z. Ling, K.A. Mahmoud, Y. Gogotsi, Charge- and size-selective ion sieving through Ti3C2Tx MXene membranes, J. Phys. Chem. Lett. 6 (2015) 4026–4031.

[19] R.J. Smith, P.J. King, M. Lotya, C. Wirtz, U. Khan, S. De, A. O'Neill, G.S. Duesberg, J.C. Grunlan, G. Moriarty, J. Chen, J. Wang, A.I. Minett, V. Nicolosi, J.N. Coleman, Large-scale exfoliation of inorganic layered compounds in aqueous surfactant solutions, Adv. Mater. 23 (2011) 3944–3948.
[20] H.S. Matte, A. Gomathi, A.K. Manna, D.J. Late, R. Datta, S.K. Pati, C.N. Rao, MoS2 and WS2 analogues of graphene, Angew. Chem. Int. Ed. Eng. 49 (2010) 4059–4062.
[21] K.G. Zhou, N.N. Mao, H.X. Wang, Y. Peng, H.L. Zhang, A mixed-solvent strategy for efficient exfoliation of inorganic graphene analogues, Angew. Chem. Int. Ed. Eng. 50 (2011) 10839–10842.
[22] J. Kibsgaard, Z. Chen, B.N. Reinecke, T.F. Jaramillo, Engineering the surface structure of MoS2 to preferentially expose active edge sites for electrocatalysis, Nat. Mater. 11 (2012) 963–969.
[23] G.D. Kang, Y.M. Cao, Development of antifouling reverse osmosis membranes for water treatment: a review, Water Res. 46 (2012) 584–600.
[24] Y. Li, S. Li, K. Zhang, Influence of hydrophilic carbon dots on polyamide thin film nanocomposite reverse osmosis membranes, J. Membr. Sci. 537 (2017) 42–53.
[25] J.N. Coleman, M. Lotya, A. O'Neill, D. S., P.J. Bergin, U. King, K. Khan, A. Young, S. Gaucher, R.J. De, I.V. Smith, S.K. Shvets, G. Arora, H.Y. Stanton, K. Kim, G.T. Lee, G.S. Kim, T. Duesberg, J.J. Hallam, J.J. Boland, J.F. Wang, J.C. Donegan, G. Grunlan, A. Moriarty, R.J. Shmeliov, J.M. Nicholls, E.M. Perkins, K. Grieveson, D.W. Theuwissen, P.D. McComb, V. Nicolosi Nellist, Two-dimensional nanosheets produced by liquid exfoliation of layered materials, Science 331 (2011) 568–571.
[26] B. Radisavljevic, A. Radenovic, J. Brivio, V. Giacometti, A. Kis, Single-layer MoS2 transistors, Nat. Nanotechnol. 6 (2011) 147–150.
[27] Y. Shi, J.K. Huang, L. Jin, Y.T. Hsu, S.F. Yu, L.J. Li, H.Y. Yang, Selective decoration of au nanoparticles on monolayer MoS2 single crystals, Sci. Rep. 3 (2013) 1839.
[28] W. Hirunpinyopas, E. Prestat, S.D. Worrall, S.J. Haigh, R.A.W. Dryfe, M.A. Bissett, Desalination and nanofiltration through functionalized laminar MoS2 membranes, ACS Nano 11 (2017) 11082–11090.
[29] C. Backes, N.C. Berner, X. Chen, P. Lafargue, P. LaPlace, M. Freeley, G.S. Duesberg, J.N. Coleman, A.R. McDonald, Functionalization of liquid-exfoliated two-dimensional 2H-MoS2, Angew. Chem. Int. Ed. Eng. 54 (2015) 2638–2642.
[30] J. Shen, Y. He, J. Wu, C. Gao, K. Keyshar, X. Zhang, Y. Yang, M. Ye, R. Vajtai, J. Lou, P.M. Ajayan, Liquid phase exfoliation of two-dimensional materials by directly probing and matching surface tension components, Nano Lett. 15 (2015) 5449–5454.
[31] R.J. Smith, P.J. King, M. Lotya, C. Wirtz, U. Khan, S. De, A. O'Neill, G.S. Duesberg, J.C. Grunlan, G. Moriarty, J. Chen, J. Wang, A.I. Minett, V. Nicolosi, J.N. Coleman, Large-scale exfoliation of inorganic layered compounds in aqueous surfactant solutions, Adv. Mater. 23 (2011) 3944–3948.
[32] W. Qiao, S. Yan, X. He, X. Song, Z. Li, X. Zhang, W. Zhong, Y. Du, Effects of ultrasonic cavitation intensity on the efficient liquid-exfoliation of MoS2 nanosheets, RSC Adv. 4 (2014) 50981–50987.
[33] V. Freger, Nanoscale heterogeneity of polyamide membranes formed by interfacial polymerization, Langmuir 19 (2003) 4791–4797.
[34] S. Karan, Z. Jiang, A.G. Livingston, Membrane filtration. Sub-10 nm polyamide nanofilms with ultrafast solvent transport for molecular separation, Science 348 (2015) 1347–1351.
[35] X. Kong, Z.-L. Qiu, C.-E. Lin, Y.-Z. Song, B.-K. Zhu, L.-P. Zhu, X.-Z. Wei, High permselectivity hyperbranched polyester/polyamide ultrathin films with nanoscale heterogeneity, J. Mater. Chem. A 5 (2017) 7876–7884.
[36] G. Eda, H. Yamaguchi, D. Voiry, T. Fujita, M. Chen, M. Chhowalla, Photoluminescence from chemically exfoliated MoS2, Nano Lett. 11 (2011) 5111–5116.
[37] A.F. Faria, C. Liu, M. Xie, F. Perreault, L.D. Nghiem, J. Ma, M. Elimelech, Thin-film composite forward osmosis membranes functionalized with graphene oxide–silver nanocomposites for biofouling control, J. Membr. Sci. 525 (2017) 146–156.
[38] J. Duan, Y. Pan, F. Pacheco, E. Litwiller, Z. Lai, I. Pinnau, High-performance polyamide thin-film-nanocomposite reverse osmosis membranes containing hydrophobic zeolitic imidazolate framework-8, J. Membr. Sci. 476 (2015) 303–310.
[39] B.-H. Jeong, E.M.V. Hoek, Y. Yan, A. Subramani, X. Huang, G. Hurwitz, A.K. Ghosh, A. Jawor, Interfacial polymerization of thin film nanocomposites: a new concept for reverse osmosis membranes, J. Membr. Sci. 294 (2007) 1–7.
[40] H. Huang, X. Qu, H. Dong, L. Zhang, H. Chen, Role of NaA zeolites in the interfacial polymerization process towards a polyamide nanocomposite reverse osmosis membrane, RSC Adv. 3 (2013) 8203.
[41] J. Yin, E.-S. Kim, J. Yang, B. Deng, Fabrication of a novel thin-film nanocomposite (TFN) membrane containing MCM-41 silica nanoparticles (NPs) for water purification, J. Membr. Sci. 423-424 (2012) 238–246.
[42] H. Dong, L. Zhao, L. Zhang, H. Chen, C. Gao, W.S. Winston Ho, High-flux reverse osmosis membranes incorporated with NaY zeolite nanoparticles for brackish water desalination, J. Membr. Sci. 476 (2015) 373–383.
[43] A.E. Childress, M. Elimelech, Effect of solution chemistry on the surface charge of polymeric reverse osmosis and nanofiltration membranes, J. Membr. Sci. 119 (1996) 253–268.
[44] H.M. Hegab, Y. Wimalasiri, M. Ginic-Markovic, L. Zou, Improving the fouling resistance of brackish water membranes via surface modification with graphene oxide functionalized chitosan, Desalination 365 (2015) 99–107.
[45] M. Safarpour, A. Khataee, V. Vatanpour, Thin film nanocomposite reverse osmosis membrane modified by reduced graphene oxide/TiO 2 with improved desalination performance, J. Membr. Sci. 489 (2015) 43–54.
[46] M. Safarpour, A. Khataee, V. Vatanpour, Thin film nanocomposite reverse osmosis membrane modified by reduced graphene oxide/TiO2 with improved desalination performance, J. Membr. Sci. 489 (2015) 43–54.
[47] W. Choi, J. Choi, J. Bang, J.H. Lee, Layer-by-layer assembly of graphene oxide nanosheets on polyamide membranes for durable reverse-osmosis applications, ACS Appl. Mater. Interfaces 5 (2013) 12510–12519.